Desaturation and structures relationships around drifts excavated in the well-compacted Tournemire's argillite and their impact on the hydraulic head profiles

Jean-Michel Matray, Sébastien Savoye, Justo Cabrera

Desaturation and structures relationships around drifts excavated in the well-compacted Tournemire's argillite and their impact on the hydraulic head profiles

Jean Michel Matray [*], Sébastien Savoye, Justo Cabrera

IRSN, DEI/SARG - BP17- 92262 Fontenay-Aux-Roses, France

[*] Corresponding Author tel 33 1 58 35 99 05 mel jean-michel.matray@irsn.fr

Abstract

This study aimed to explore the relationships between the rock desaturation and the EDZ extension subsequent to the excavation of a century-old tunnel and recent drifts (1996 and 2003) at the Tournemire Underground Research Laboratory. The other objective of this work was to assess the impact of this desaturation on the hydraulic head profile measured around the tunnel. One section was selected per drift. Two boreholes were realized for each section: parallel and inclined (45°) with respect to the bedding. For each borehole, we performed on-site drill core mapping, petrophysical measurements and pneumatic and hydraulic tests by means of a Modular Mini-Packer System (MMPS) device.

Results indicate that EDZ around drifts is mainly a combination of unloading joints, mimicking the drift shape, and of desaturation cracks, parallel to the bedding. The EDZ extension around the tunnel is twice to three times that of drifts 1996 and 2003 and essentially composed of unloading joints resulting from the mechanical response of the rock. The masonery covering the tunnel walls is assumed to have protected the rock from the seasonal variations of the air humidity, thus limiting (without excluding) the formation of desaturation cracks. The EDZ extension deduced from core mapping is in agreement with that deduced from pneumatic tests with permeabilities several orders of magnitude greater than in the undisturbed zone. Degrees of saturation for the three sections range between 0.9 and 1 in the EDZ area and reach 1 in the undamaged zone. The head profile deduced from measurements recorded since 2002 indicates the occurrence of sub-atmospheric water pressures with an extension of *ca* 40m around the tunnel. We have searched to quantify the impact of the tunnel since its excavation on the degrees of saturation and the hydraulic heads. The simulation was performed by

considering, as a first approach, the absence of fracturation in the EDZ area. A constant suction of -3300m, deduced from the mean annual values of relative humidity and temperature measured in the tunnel atmosphere since 2002, was applied at the tunnel wall. The degrees of saturation simulated around the tunnel are underestimated in the EDZ area and consistent to experimental data in the unfractured zone. The modelling of hydraulic heads is quite consistent to experimental values in the vertical direction and overestimated in the horizontal direction.

This study has demonstrated the role played by fracturation on the distribution of petrophysical parameters and of heads around drifts and the century-old tunnel. It has also demonstrated the necessity of coupling mechanic and hydraulic calculations by considering capillary forces.

Key words: Tournemire, argillite, permeability, EDZ, desaturation

40 ## 1. Introduction

41 Argillaceous formations are considered in several European countries as potential
42 repository host rocks for high-level radioactive wastes in deep geological
43 formations. Their very low water velocity (due to a very low permeability and
44 diffusivity and a moderately low hydraulic gradient) coupled to a large thickness
45 (several hundreds of meters) and a high sorption capacity make these rocks
46 potentially interesting for a repository as radionuclide transfer times should exceed
47 several times the radionuclide half-lives. However, construction of a repository can
48 lead to perturbations due to excavation works and the subsequent decompression
49 of the surrounding rocks, ventilation of the underground drifts or construction of
50 the engineered barriers. Host rock properties around structures (tunnel, drifts and
51 niches) are likely altered during and after excavation works. Plastic deformations
52 are especially expected in an altered zone called excavation disturbed zone (EDZ),
53 depending on the mechanical properties, the initial stress field and excavation
54 techniques (Bossart et al., 2002). A fracture network consisting in unloading
55 fractures and of desaturation cracks is developed in this EDZ with hydraulic
56 conductivities orders of magnitude higher than those of the unaltered zone. This
57 fracture network can thus facilitate the transfer of radionuclides towards the
58 biosphere along galleries and shafts in case of radionuclide release from waste
59 containers and tightness default of engineered barriers. It can also modify the
60 petrophysical properties of the claystone around the structure network. Porosity
61 and water content are amongst the most sensitive properties due to the relaxing of
62 constraints and to hydration/dehydratation cycles under low humidity conditions
63 (Charpentier et al., 2003). Ventilation of the underground drifts and shafts during
64 the construction and the operation phases can induce the partial desaturation of

65 the rock around the drift, thus modifying its thermo hydro-mechanical properties
66 (Mayor et al., 2005). This change in the rock properties affect a zone around
67 excavations called Excavation disturbed Zone (EdZ) which may have an impact on
68 the design of the potential repository (drift spacing and repository size). One of the
69 greatest disturbance concerns the distribution of the hydraulic profiles around
70 excavations.
71 To evaluate the impact of excavations, and more particularly, of desaturation on
72 the hydraulic and petrophysical properties of a claystone, the French Institute of
73 Radioprotection and Nuclear Safety (IRSN) has been conducting research
74 programmes since 1991 in its underground research laboratory of Tournemire, in
75 the Aveyron country (south of France). The Tournemire URL crosses a Toarcian
76 argillaceous formation *via* a century-old tunnel and its adjacent drifts excavated in
77 1996 and in 2003. The tunnel and drifts are naturally ventilated since their
78 excavation with mean annual relative humidity less than 100% and likely
79 responsible of the partial desaturation of the rock (Ramambasoa, 2001, Valès et
80 al., 2004).
81 This paper aims to characterize the extent of desaturation around the different
82 structures (tunnel and drifts) of the URL and to understand the role of this
83 desaturation on the petrophysic and hydraulic properties of the rock.
84 Characterization has been performed by means of 6 cored boreholes, with 2
85 boreholes per structure (century old tunnel, drift 1996 and drift 2003), one parallel
86 to the bedding and the second with a dip angle of 45°down at the intersection of
87 the drift and the ground to access the area assumed to be most fractured of the
88 EDZ but also for assessing the time and structure-shape dependency on
89 desaturation. For each drift and tunnel, these boreholes have been analyzed for

90 their structures (unloading and tectonic joints), petrophysical properties (total
91 porosity, gravimetric water content, degree of saturation and volumetric moisture
92 content). In parallel, each of these boreholes has been tested for determining their
93 permeabilities by means of pneumatic and hydraulic tests.
94 The role of this desaturation on the petrophysical and hydraulic properties of rock
95 around structures is then assessed by comparing the hydraulic heads estimated
96 around the tunnel after in situ pressure measurements to hydraulic heads obtained
97 from a numerical simulation performed since the tunnel excavation. This
98 preliminary modelling was performed without taking into account mechanical
99 aspects, by means of VS2DT 3.0, a computer program developed by the U.S.
100 Geological Survey for solving problems of water flow and solute transport in
101 variably saturated porous media.
102
103 **2. Geological, structural and hydrogeological background**
104
105 The Tournemire URL is located in a Mesozoic marine basin on the southern border
106 of the French *Massif Central* and at the western limit of the *Causse du Larzac*. The
107 studied argillaceous formation is a 250m-thick and corresponds to sub-horizontal-
108 indurated argillaceous and marly layer of Toarcian and Domerian age (Fig. 1). This
109 formation is sandwiched between two carbonated and karstified aquifers.
110 The Tournemire *massif* is a monocline structure with a mean dip angle of about -4°
111 to the North. The lower (Hettangian to Carixian series) and upper (Aalenian to
112 Bathonian series) aquifers are 300m and 250m thick, respectively and essentially
113 composed of limestone and dolomite. The argillaceous formation is composed of
114 250m of well-compacted and thinly bedded claystones and marls. The clay fraction

115 is ranging between 20 and 50% of the bulk rock. It is mainly composed of illite (5 to
116 15%), illite/smectite mixed-layer minerals (5 to 10% with a smectitic proportion of
117 about 10%), chlorite (1 to 5%) and kaolinite (15-20%). The claystone also contains
118 10 to 20% of quartz grains, 10 to 40% of carbonates (mainly composed of calcite
119 with traces of dolomite and siderite) and 2 to 7% of pyrite (Cabrera et al., 2001;
120 Savoye et al., 2001; Savoye et al., 2006).
121 The upper Toarcian is crossed by a 1885m long and century-old railway tunnel
122 excavated between 1882 and 1886. This tunnel was an excellent opportunity to
123 IPSN (now IRSN) to have an easy access to an argillaceous formation and develop its
124 own research programmes for training its experts in evaluating the possibilities and
125 processes of radionuclide transport in such kind of rocks.
126 The Tournemire massif is separated by a reverse and very transmissive major
127 structure namely the Cernon fault (80km long). This fault is oriented West-East and
128 enables the communication between the two aquifers. The massif is also affected
129 by secondary faults of hectometric extension and oriented NW to SE. These
130 fractures are generally filled with calcite and give access to unfractured blocks in
131 argillites characterized by hydraulic conductivities amongst the smallest in the
132 world (between 10^{-14} and 10^{-15} m/s *i.e.* 10^{-21} and 10^{-22} m^2 as intrinsic permeabilities)
133 for a storativity of *ca* 10^{-6} (Boisson et al., 1998; Cabrera et al., 2001). Secondary
134 faults sometimes present geodic cavities in relay zones that enable the vertical
135 transfer of fluids. With the Cernon fault, these fractures are the only opportunity
136 of getting fluids in contact with the clay formation. Hydraulic test performed on
137 these relay structures have supplied relatively high transmissivities (around 10^{-10}
138 m^2/s) *i.e.* with permeabilities orders of magnitude higher than those of the
139 unfractured zone and for an equivalent tested height (Savoye et al., 2003). Fig. 2

shows the distribution of the stabilized hydraulic heads with respect to boreholes CA and DC located in the tunnel axis. Pressures have been measured in the unfractured zone with permanent sealed probes (boreholes PH1 and PH3) and a multipacker system (borehole PH2) and in the water-bearing fractures by means of double packer devices (boreholes TN2, M2 and ID180). Fig. 2 shows a depression of *ca* 30m around the tunnel with respect to the hydrostatic profile drawn from heads measured in the two aquifers (H_{CA} = 583m NGF and H_{DC}= 453m NGF). This region is characterized by the occurrence of sub-atmospheric water pressures and constitutes a capillary fringe (Horseman et al., 1996) around the tunnel as a consequence of its excavation and natural ventilation. On the contrary, the hydraulic head measured in a 80m height test section in the lower part of the argillaceous formation and isolating a water-bearing fracture likely indicates the occurrence of an overpressure in the argillite.

Two other fracture networks exist at the Tournemire URL that may have an important role on water flow and transport of dissolved species. These networks are essentially confined around the tunnel and drifts. The first one is due to the stress redistribution during excavation and subsequent rock convergence. It consists in a combination of unloading joints and fractures namely excavation disturbed zone (EDZ). The second network is made of subhorizontal fractures at the drift wall and developed parallel to the bedding (several meters deep each with a millimetric aperture and a frequency of about 1 per 10cm). This network is directly linked to seasonal variations of the drifts atmosphere (hygrometry and temperature) and attributed to variations in the chemical potential of the interstitial solutions under swelling/shrinking cycles (Ramambasoa, 2001, Valès et al., 2004). Indeed, the drift hygrometry recorded since 1999 indicates seasonal

variations (40% RH and 8°C in winter and 100% and 14°C in summer) with a mean annual RH value of 77% leading to a partial evaporation of the interstitial water. There is a clear correlation between this network aperture and hygrometry with a lag time of about 60h between the fracture aperture recorded by means of extensometers and RH variations measured with capacitive thermohygrometers (Fatmi et al., 2004).

3. Materials and Methods

3.1 Realization of boreholes

Six boreholes with length ranging between 1 and 6 meters were air-drilled between June 2004 and February 2005 from the tunnel and the experimental drifts excavated in 1996 and 2003. Boreholes were realized with an Hilti device and supplied core samples of about 35 cm long each with a diameter of 55mm. Boreholes locations are shown in Fig. 3 and their main characteristics summarized in Table 1.

3.2 Drill core mapping

The core analysis and pictures were performed immediately after their removal from boreholes and just before the plug preparation for petrophysical measurements. A thorough structural analysis reported on core unrolling was performed trying to distinguish between fracturation related to the excavation works and the subsequent desaturation to that induced by tectonic events.

190

191 *3.3 Petrophysical measurements by water content and volume determinations*

192

193 Immediately after, the cores were entirely sawed on-site in plugs 3-4cm long each
194 for their 105/150°C-water content and volume measurements with the goal of
195 determining the following parameters: total porosity, volumetric moisture content,
196 gravimetric water content and degree of saturation as a function of the distance
197 from the borehole head. The total mass of the humid samples (M_{tot}) was measured
198 right after sawing. Then, the total apparent volume of the humid samples (V_{tot}) was
199 determined following the method detailed in Monnier et al. (1973) that uses
200 Archimedes'principle by weighing the displacement of petroleum (kerdane) with a
201 Sartorius YDK 01 density measurement kit. This determination has required i) to
202 saturate sample in petroleum just after the M_{tot} measurement, ii) the
203 determination of the relationship between the kerdane density and temperature
204 iii) plus additional measurements among which the mass of humid sample in the air
205 after saturation in oil (W_a) and the sample mass after immersion in petroleum (W_p).
206 The plugs were then oven dried at 105°C and 150°C until stabilization (*i.e.* after 2
207 to 4 days for each temperature) for measuring their respective masses $M_{105°}$, $M_{150°}$.
208 All masses were determined on-site with the same accurate scale (OHAUS, type
209 Adventurer AR3130 having a repeatability of 0.001g for masses ranging between 0
210 and 310g). The grain density (ρ_s) was obtained by He-pycnometry with a mean
211 value of 2.704 g.cm^{-3} at 105°C and 2.703 g.cm^{-3} at 150°C for a standard deviation
212 of 0.004 g.cm^{-3}. The water density (ρ_W) was calculated from an estimation of the
213 interstitial water to 1.0012 g.cm^{-3} with a standard deviation of 0.0004 g.cm^{-3}. The
214 definitions of functions are those reported in Pearson et al. (2003). The total or

physical porosity (n_{tot}, dimensionless) is the ratio of the pore volume to total apparent volume ($n_{tot} = V_{pores}/V_{tot}$ with $V_{pores} = V_{tot} - V_{solids} = V_{tot} - M_{105°/150°}/\rho_{s105°/150°}$ where $\rho_{s105°/150°}$ is the grain density obtained at 105°C or 150°C). The gravimetric water content, dry mass basis ($WC_{dry,105or150°}$, dimensionless) is the ratio of the mass of water (M_W=M_{tot}-$M_{105°}$ where M_{tot} represents the total mass of the humid sample) and the oven dry mass $M_{105°}$ or M_{150} such as $WC_{dry,105or150°} = 100 \times (M_w / M_{105or150°})$. The degree of saturation (S, dimensionless) is the ratio of water-filled to total pore space ($S = (V_W / V_{pores})$ with $V_w = (M_{tot} - M_{105/150°})/\rho_W$). The volumetric moisture content (θ, dimensionless) is the ratio of water-filled pore space to total volume (V_w/V_{tot}) and becomes a function of the degree of saturation (S) and of total porosity such as: $\theta = Sr \times n_{tot}$.

In addition, there was some SEM observations performed at IRSN for verification of the occurrence or absence of heavy minerals like pyrite and lighter minerals like carbonates which have an important impact on the grain density of samples.

Errors on functions U = F(V1, V2, …) were estimated by propagation of the analytical errors variances following the classical Gauss formula ($\sigma_U^2 = \sigma_{V1}^2 (\partial F/\partial V)^2 + \sigma_{V2}^2 (\partial F/\partial V)^2 + \ldots$ *in* Theoria combinationis, 1821).

3.4 Pneumatic and hydraulic tests

The MMPS (Modular Mini-Packer System) equipment was initially designed for hydraulic testing in the excavation disturbed zone of the Mont Terri Laboratory (Cottour et al., 1999). It allows up to five individual packer modules with a diameter of 52 mm to be coupled in a variety of configurations. Each packer

239 module consists in a stand-alone unit with a packer inflation line and both flow and
240 pressure measurement lines. Packer pressures are controlled by a manometer
241 installed at the control unit, while both a manometer and a pressure transducer
242 control interval pressures. The configuration of the MMPS is shown in the Fig. 4. A
243 series of four 10.5 cm intervals separated through four 10 cm packers were
244 applied. Beyond, a 100 cm packer and a last 10 cm packer located at the bottom of
245 the MMPS were installed such that a fifth 10.5-cm interval (Fig. 4) allows a less
246 disturbed zone to be simultaneously characterized. Use of 1-m length extension
247 tubes permit an area up to 5m (in the tunnel boreholes) to be investigated.
248 Pneumatic tests were performed prior to hydraulic testing to provide an estimate
249 of both the extent and the connectivity of the fracture network and also semi-
250 quantitative estimates of interval permeability of the tested intervals.

251 *Pneumatic testing*

252 Pneumatic tests have already been performed in consolidated argillaceous rocks in
253 the Mont Terri's URL with the aim of characterizing the EDZ extension (Bossart et
254 al., 2002). They consist in injecting nitrogen or pumping air in/out of the interval
255 and in interpretating the corresponding pneumatic response with the MMPS device.
256 The surface test equipment allows working with injection and extraction flow rates
257 between 0.1 and 50 l/min at standard conditions.

258 The MMPS was set into the boreholes immediately after their realization. Packers
259 were inflated to 20 to 25 bars to limit the possibility of packer bypass. Afterwards,
260 during the injection of nitrogen or the extraction of air using a vacuum pump, the
261 air flow rates and the pressures in the test and observation intervals were recorded
262 with a data acquisition system. A test was stopped when steady-state conditions
263 were either reached or the pressure and flow rate measurements indicated a

permeability below the detection limit of about 5×10^{-17} m^2. The detection limit was reached when flow rates dropped below the measurement limit during air extraction tests or when pressures during injection tests were completely dominated by wellbore storage effects. The estimate of gas permeability was deduced from a steady state approximation of pneumatic test data as described in details by Bossart et al. (2002).

Hydraulic testing

They were performed right after pneumatic testing either in intervals showing values of gas permeability under the detection limit, thus indicating that rock should be water-saturated without occurrence of connected fractures, or in intervals crossing a very transmissive single fracture to verify estimates from pneumatic tests as in borehole MD6. In the former case, intervals were just filled with synthetic water and pulse-tests were applied. In the second case, the single fracture was first artificially saturated by means of a circulation of synthetic water. Then, a hydraulic cross-hole test was performed by injecting water at a constant overpressure of approximately 2m.

The pulse test data were analyzed using the method developed by Bredehoeft and Papadopoulos (1980) and the constant head injection test using a straight line analysis (Jacob and Lohman, 1952) on a pressure *vs* log time plot (see Bossart et al., 2002 for details).

4. Results

288 All data are shown for each section in Fig. 5 to Fig. 7 as a function of the distance
289 from the borehole head. Each figure reports results obtained on the two boreholes
290 of a same section (A for drift 2003, B for drift 1996 and C for the century-old
291 tunnel). For each borehole, are given the drillcore mapping showing the extension
292 of the EDZ, the degree of saturation calculated from petrophysical measurements
293 of sample volumes and masses for samples oven dried at 150°C and permeabilities
294 determined from pneumatic and hydraulic tests. The average petrophysical
295 properties determined inside and outside the EDZ areas are summarized in Table 2.
296
297 *4.1 Section A (drift 2003)*
298
299 The drillcore mapping shows a destructured (DZ) Excavation Disturbed Zone (EDZ)
300 with an extension of about 30cm and 50cm in MD2 (horizontal) and MD4 (inclined),
301 respectively. Those destructured zones are characterized by a High Density
302 Fracturation (HDF) combining unloading joints (UJ), mimicking the gallery shape,
303 and desaturation cracks (DC), parallel to the bedding. Borehole MD2 also shows the
304 occurrence of isolated unloading joints at distances of about 40 and 70cm and of a
305 water-bearing mechanical fracture (MF) capturing water from fractures of tectonic
306 origin. One calcite-filled microfracture of tectonic origin is also observed in MD4.
307 Table 1 shows that petrophysical parameters inside the EDZ are systematically
308 lower than outside. Both boreholes show a desaturation trend in the destructured
309 zones with values increasing from 95% in MD4 and 98% in MD2 at the borehole head
310 up to about 100% close to the EDZ outer border with an error of ca 3%. Outside the
311 EDZ, the rock may be considered as fully saturated. There are also two kinds of
312 artefacts. The first one is artificial and refers to strong desaturation trends at the

313 core limits as a consequence of an overheating during the *in situ* core break and
314 removal. The second type is natural and attributed to the presence or default of
315 heavy minerals like pyrite (density of 5). Degrees of saturation greater than one as
316 shown in MD4 are attributed to the second type after SEM observations.
317 The permeability profiles obtained from pneumatic tests show a progressive
318 decrease of values which are very high ($\geq 10^{-12}$ m^2) in the EDZ areas to very low
319 values ($\leq 10^{-17}$ m^2) in the undisturbed zones. The extent of the partially-saturated
320 zone is greater for MD2 than for MD4 and is explained by the presence of unloading
321 joints up to about 70cm from the borehole border in MD2. Hydraulic tests
322 performed in the water-bearing fracture crossed in MD2 indicate a permeability of
323 *ca* 10^{-14} m^2.
324
325 *4.2 Section B (drift 1996)*
326
327 There is a bigger EDZ extension in MD3 (horizontal) than in MD5 (inclined). This
328 result is due by a bigger extension of desaturation cracks reaching *ca* 45cm and
329 30cm in MD3 and MD5, respectively. On the contrary, the EDZ unloading joints are
330 limited to the very first 20cm in MD3 with a high density fracturation and reach up
331 to 35cm in MD5 with a low density fracturation. Both boreholes also show the
332 occurrence of tectonic microfractures filled with calcite.
333 As in section A, the mean values of petrophysical parameters (Table 2) are
334 systematically lower inside the EDZ than outside. There is no clear desaturation
335 trend in MD3 but values as low as 94% are calculated up to about 80cm. On the
336 contrary, borehole MD5 shows a clear desaturation profile limited to the EDZ
337 extent. In both boreholes the border artefacts are observed as in section A.

338 The permeability profile obtained from pneumatic tests performed in MD3 shows a
339 progressive decrease of values from ≥ 10^{-11} m^2 in the very first 60cm down to ≤10^{-17}
340 m^2 at about 2m, *i.e.* far away from the EDZ extension. The presence of tectonic
341 fractures filled with calcite could explain this behaviour. Permeabilities obtained in
342 MD5 are much more lower (10^{-16}< k m^2 < 10^{-15}) than for MD3. This behaviour is quite
343 similar to that observed in the inclined borehole MD4 from section A. An hydraulic
344 tests was performed in the saturated area at 2.3m from the borehole head and
345 gave a permeability of about 10^{-18} m^2, *i.e.* very close to that determined from
346 pneumatic tests at the same distance (10^{-17} m^2).
347
348 *4.2 Section C (century-old tunnel)*
349
350 The drillcore mapping shows an EDZ of about 1m in both MD6 (horizontal) and MD7
351 (inclined). High density fracturation of unloading joints concerns the whole EDZ in
352 MD6 and only the first 50cm in MD7. The EDZ unloading joints observed in MD7 also
353 show the occurrence of gypsum spots.
354 Table 2 shows that the MD6 petrophysical parameters are systematically lower
355 inside the EDZ than outside. MD7 shows the inverse situation but uncertainties
356 calculated for this borehole are so important that the real behavior may be
357 overwhelmed by errors.
358 The permeability profiles obtained from pneumatic tests performed in MD6 and
359 MD7 show very high permeabilities in the High Density Fracturation zones with
360 values ranging between 10^{-13} and 10^{-12} m^2. An attempt of artificial saturation of this
361 zone has allowed the conduction of an hydraulic test giving a permeability

362 estimation of about 10^{-11} m^2, *i.e.* very close to those estimated from pneumatic
363 tests. Permeabilities calculated out of these areas are less 10^{-17} m^2.
364
365 **5. Discussion**
366
367 *5.1 EDZ and desaturation extensions*
368
369 The study of the fracture network from the drillcore mapping shows that the
370 extension of the EDZ at the Tournemire URL is a combination of unloading joints
371 and of desaturation cracks. This extension is bigger around the tunnel (*ca* 1m in
372 both boreholes MD6 and MD7) than around drift 1996 (up to 45cm from the
373 horizontal MD3 and 30cm from the inclined MD5) which in turn shows a bigger
374 extension than around drift 2003 (around 30 cm in the horizontal borehole MD2 and
375 up to 40cm in the inclined MD4). Desaturation cracks are not visible around the
376 tunnel contrary to drifts. The masonery made of limestone blocks (70-80cm thick)
377 and covering the tunnel wall since the end of excavation works is likely protecting
378 the rock from the natural ventilation of the tunnel and could therefore explain the
379 lack of desaturation cracks around the tunnel. The uncovered drifts show the
380 occurrence of desaturation cracks with a bigger extension in horizontal boreholes
381 (MD3 and MD2) than in the inclined one (MD4 and MD5) as a consequence of cracks
382 developed along the subhorizontal bedding planes. The extension of unloading
383 joints decreases with the age of the structure (tunnel, drifts) and is generally
384 bigger in inclined boreholes compared to the horizontal one. Therefore, a time-
385 dependency on the EDZ unloading joints extension is suggested.

386 The permeability profiles determined from pneumatic and hydraulic tests perfectly
387 fit the EDZ extension. Permeabilities are the highest (between 10^{-11} and 10^{-12} m^2)
388 into the High Density Fracturation and Destructured Zones of the EDZ. They
389 progressively decrease in the Low Density fracturation area to reach the values
390 inferior to 10^{-17} m^2 in the undisturbed zone of the EDZ.
391 There is also a strong correlation between the desaturated area determined from
392 petrophysical determinations with the extension of the EDZ deduced from the
393 coupled study of the core mapping and of permeability measurements. With the
394 exception of borehole MD7, all petrophysical parameters determined inside the EDZ
395 are systematically lower than outside. The degree of saturation reflects the
396 evolution of the water content and total porosity which are clearly linked to the
397 extent of the EDZ fracturation. Therefore, the lower porosities and water content
398 determined in the EDZ are likely a consequence of unloading and capillary coupled
399 forces.
400
401 *5.2. Modelling of saturation profiles and hydraulic heads around the tunnel*
402
403 The main objective of this preliminary modelling is to *assess* the capability of a
404 Richard's desaturation model to reproduce both desaturation and pressure head
405 data measured around the tunnel. In the Richard's model (de Marsily, 1986; Genty
406 et al., 2002), both water submitted to gravity and suction forces are taken into
407 account. The Richard's equation is solved with a finite difference formulation
408 implemented in VS2DTI 3.0 code (Lappala et al., 1983; Hsieh et al., 1999). The
409 fracturation observed in the EDZ is not considered here. Model input data are
410 porosity n_{tot}, suction curves giving the relationship between saturation S_w and

411 suction ψ expressed as a function of the pressure head h, permeability K expressed
412 as a product of the saturated permeability K_s and the relative permeability curve K_r
413 function of the pressure head. Expression of $S_w(h)$ and $K_r(h)$ given below, were
414 formulated following the van Genuchten model (van Genuchten, 1980), as follows:

415 $$S_e = \frac{1}{(1+|\alpha h|^{\beta})^{1-\frac{1}{\beta}}}$$

416 $$k_r = \left\{1-|\alpha h|^{(\beta-1)}(1+|\alpha h|^{\beta})^{(\frac{1}{\beta}-1)}\right\}\sqrt{(1+|\alpha h|^{\beta})^{(\frac{1}{\beta}-1)}}$$

417 Where α and β are the parameters of the van Genuchten model and S_e, the
418 effective saturation expressed in terms of volumetric moisture content θ and
419 residual moisture content θ_r.

420 $$S_e = \frac{\theta-\theta_r}{n_{tot}-\theta_r}$$

421 Lab and *in situ* hydraulic tests have allowed an estimate of a mean value for
422 permeability of about 10^{-14} $m.s^{-1}$ (Boisson et al., 2001; Bertrand et al., 2002).
423 Parameters for the van Genuchten suction curve were deduced from lab data
424 obtained by Daupley (1997): α= $1.5.10^{-4}$, β= 2.5 and θ_r =0.0056. The mean value of
425 total porosity measured in this study was equal to 9% (Table 2).
426 As the purpose of the calculations is to quantify the impact of tunnel on the
427 saturation degrees and the hydraulic heads, the size of the simulated zone must
428 also include domains out of the tunnel's influence. Thus, the 2D mesh consists in a
429 60mx120m rectangle in which a half tunnel is equidistant to the top, bottom and
430 right side of the domain. The hydraulic boundary conditions were of the form: i)
431 hydrostatic conditions imposed by the two surrounding aquifers were applied at the
432 upper and lower limits; ii) a constant suction (-3300m) was imposed at the tunnel

433 wall. The capillary pressure value was derived from the temperature and relative
434 humidity variations (Ramambasoa, 2001; Valès et al., 2004) measured in the tunnel
435 using the Kelvin's equation; iii) a no-flow-boundary was applied at the others
436 limits. The initial time for simulation is the year 1888, corresponding to the end of
437 the tunnel excavation.
438 Fig. 8 (a)-(b) compares the degrees of saturation simulated along boreholes MD6
439 and MD7 to values calculated from petrophysical data. Modelling results are roughly
440 consistent to experimental data except in the EDZ where they are slightly lower.
441 This discrepancy suggests that our single porosity model is likely smoothing the
442 heterogeneities induced by the occurrence of fractures. The comparison between
443 the simulated and the measured hydraulic heads is given in Fig. 9 (a)-(b). The
444 modelling of hydraulic heads in the vertical direction is quite consistent with those
445 measured in PH1 and PH3, despite the lack of in situ measurements at
446 intermediate level. In the horizontal direction, the discrepancy between the
447 simulated and the in situ values, especially in the deepest level, suggests that the
448 influence of tunnel would be greater than that derived from modelling. The
449 presence of a high density fracturation made of unloading joints resulting from the
450 mechanical response of the rock to the present field of constraints or/and to the
451 re-use of weakness plane of an ancient tectonic event could explain the occurrence
452 of a capillary fringe around the tunnel. This fracturation is assumed to have
453 increased the penetration depth of the suction effect and explains that the
454 measured hydraulic heads are less than the simulated one. The extension of this
455 depression may reach several tens of metres around the tunnel and makes part of
456 the Excavation disturbed Zone (EdZ). A new modelling considering hydromechanical
457 coupled processes is actually in progress with the aim of simulating the EDZ

458 formation. The comparison of modellings performed in the framework of this paper
459 to the hydromechanical coupled one will help to verify the role played by
460 desaturation cracks on the hydraulic head profiles.
461
462 **6. Conclusion**
463 The purpose of this study was twice. Firstly, to explore the relationships between
464 the rock desaturation subsequent to the excavation of a century-old tunnel and of
465 modern drifts (1996 and 2003) and the EDZ extension. Secondly, to assess the
466 impact of this desaturation on the hydraulic head profile measured around the
467 tunnel and the drifts. One section was selected per structure (drift 2003, drift 1996
468 and century-old tunnel). We have realized two new boreholes for each section: one
469 parallel to the bedding and the other one inclined downward at 45°at the gallery
470 wall and ground intersection. For each borehole, we performed on-site drill core
471 mapping, petrophysical measurements and at last, pneumatic and hydraulic tests
472 by means of a Modular Mini-Packer System (MMPS) device.
473 Results indicate that EDZ around drifts is mainly a combination of unloading joints,
474 mimicking the drift shape, and of desaturation cracks, parallel to the bedding. The
475 EDZ extension around the tunnel is twice to three times that of drifts 1996 and
476 2003 and essentially composed of unloading joints resulting from the mechanical
477 response of the rock to the present field of constraints or to the resumption of an
478 ancient tectonic damage. The masonery covering the tunnel walls is assumed to
479 have protected the rock from the seasonal variations of the air humidity, thus
480 limiting (without excluding) the formation of desaturation cracks. The EDZ
481 extension deduced from core mapping is also in agreement with that deduced from
482 pneumatic tests with permeabilities several orders of magnitude greater than in

483 the undisturbed zone. Degrees of saturation deduced from petrophysical
484 measurements for the three sections range between 0.9 and 1 in the EDZ area and
485 reach saturation in the undamaged zone. Hydraulic heads are measured since 2002
486 by permanent pressure probes installed in the unfractured rock around the tunnel
487 and by piezometers installed in the surrounding aquifers. The head profile indicates
488 the occurrence of sub-atmospheric water pressures with an extension of *ca* 40m
489 around the tunnel. We have searched to quantify the impact of the tunnel since its
490 excavation on the degrees of saturation and the hydraulic heads. The simulation
491 was performed with the VS2DTI 3.0 code by using the Richard's desaturation model
492 and considering, as a first approach, the absence of fracturation in the EDZ area. A
493 constant suction of -3300m, deduced from the mean annual values of relative
494 humidity and temperature measured in the tunnel atmosphere since 2002, was
495 applied at the tunnel wall. The degrees of saturation simulated around the tunnel
496 are underestimated in the EDZ area and consistent to experimental data in the
497 unfractured zone. The modelling of hydraulic heads is quite consistent to
498 experimental values in the vertical direction and overestimated in the horizontal
499 direction. The occurrence of an unloading-joints fracture network resulting from
500 the mechanical response of the rock to the present field of constraints or to the re-
501 use of weakness zones of an ancient tectonic event is assumed to have created
502 very high capillary pressures in the EDZ and could therefore explain discrepancies
503 between the observed and simulated hydraulic heads.
504 This study has demonstrated the role played by fracturation on the distribution of
505 petrophysical parameters and of heads around drifts and the century-old tunnel. It
506 has also demonstrated the necessity of coupling mechanic and hydraulic

calculations by considering capillary forces. Such calculations will be performed in a next step.

Acknowledgments

The authors gratefully acknowledge S. Lemius for his help when carrying out petrophysical measurements and M. Piedevache and M. Kech from Solexperts for performing pneumatic and hydraulic testing. We also wish to give our acknowledgement to C. Combes for realizing boreholes.

514 **References**

515 Bertrand, L., Laviguerie, R., Cabrera, J., Matray, J.-M., Savoye, S., 2002.
516 Instrument for measuring pore pressure and permeability in low permeability rock.
517 International meeting "Clays in natural and engineered for radioactive waste
518 confinement", organized by ANDRA in Reims, Conference Proceeding, 321-322.

519 Boisson, J.Y., Cabrera, J., Bertrand L., Heitz, J.F., 1998. Mesures de très
520 faibles perméabilités in situ et en laboratoires sur les argilites de Tournemire
521 (Aveyron). Méthodologies comparées et effet d'échelle. Bull. Soc. Géol. France,
522 169, 595-604.

523 Boisson, J.Y., Bertrand, L., Heitz J.F., Moreau-Le Golvan, Y., 2001. In situ and
524 laboratory investigations of fluid flow through an argillaceous formation at
525 different scales of space and time, Tournemire tunnel, southern France. Hydrogeol.
526 J. 9, 108-123.

527 Bossart, P., Meier, P.M., Moeri, A., Trick, T., Mayor, J.C., 2002. Geological and
528 hydraulic characterisation of the excavation disturbed zone in the Opalinus Clay of
529 the Mont Terri Rock Laboratory. Eng. Geol. 66, 19-38.

530 Bredehoeft, J.D., Papadopoulos, S.S., 1980. A method for determining the
531 hydraulic properties of tight formations. Water Resour. Res. 16, 233-238.

532 Cabrera, J., Beaucaire, C., Bruno, G., De Windt, L. Genty, A., Ramanbasoa,
533 N., Rejeb, A., Savoye, S., Volant, P., 2001. Projet Tournemire – Synthèse des
534 programmes de recherche 1995-1999, Rapport IPSN DPRE/SERGD 01-19, Paris
535 France.

536 Charpentier, D., Tessier, D., Cathelineau, M., 2003. Shale microstructure
537 evolution due to tunnel excavation after 100 years and impact of tectonic paleo-
538 fracturing. Case of Tournemire, France. Eng. Geol. 70, 55-69.

539 Cottour, Ph., Bigarré, P., Camus, P., Bauer-Plaindoux, C., Blümling, P.,1999.
540 Evaluation of in-situ stresses. Comparison of techniques. In: M. Thury and P.
541 Bossart, Editors, *Results of the Hydrogeological, Geochemical and Geotechnical*
542 *Experiments, Performed in 1996 and 1997. Swiss National Geological and*
543 *Hydrogeological Survey. Geological Report* vol. 23, pp. 160-170.
544 de Marsily, G., 1986. Quantitative hydrogeology, Academic Press inc. (London).
545 Daupley, X., 1997. Etude du potentiel de l'eau interstitielle d'une roche
546 argileuse et des relations entre ses propriétés hydriques et mécaniques. Thèse de
547 l'Evocole Nationale Supérieure des Mines de Paris.
548 Fatmi, H., Mangin, A., Matray, J.M., 2004. Traitement et exploitation des
549 séries temporelles de pression, température et humidité obtenues sur le site de
550 Tournemire. Rapport IRSN/DEI/SARG 04-24, Paris, France.
551 Genty, A., Bassot, S., Bruno, G., Cabrera, J., Le Potier, C., 2002. Modelling of
552 desaturation experiments on Tournemire argillite samples. Poromechanics II,
553 Auriault et al. (eds.), 437-443.
554 Horseman, S.T., Higgo, J.J.W., Alexander, J., Harrington, J.F., 1996. Water,
555 gas and solute movement through argillaceous media. OECD/NEA CC-96/1:290.
556 Hsieh, P.A., Wingle, W., Healy R.W., 1999. A graphical software package for
557 simulating fluid flow and solute or energy transport in variably saturated porous
558 media. US. Geological Survey report- Water Resources Investigations N°99-4130.
559 Jacob, C.E., Lohman, S.W., 1952. Nonsteady flow to a well of constant
560 drawdown in an extensive aquifer. Trans. AGU 33 (1952), pp. 559-569.
561 Lappala, E.G., Healy, R.W., Weeks, E.P., 1983. Documentation of computer
562 program VS2D to solve the equations of fluid flow in variably saturated porous
563 media. US. Geological Survey report- Water Resources Investigations N°83-4099.

564 Mayor, JC., Garcia-Sineriz, J.L., Velasco, M., Gomez-Hernandez, J., Lloret, A.,
565 Matray, J.M., Coste, F., Giraud, A., Rothfuchs, T., Marshall, P., Fierz, T.,
566 Klubertanz, G., 2005. Ventilation Experiment in Opalinus Clay for the disposal of
567 radioactive waste in underground repositories. (Project funded by the European
568 Communnity under the 'EURATOM' Programme 1998-2002 under contract N° FIKW-
569 CT-2001-00126). EC Final Tech. Publ. Rept. CEC Nuclear Science & Technology
570 Series Luxembourg pp. 41.

571 Monnier, G., Stengel, P., Fies, JC., 1973. Une méthode de mesure de la
572 densité apparente de petits agglomérats terreux. Application à l'analyse de
573 système de porosité du sol. Ann. Agron. 24, 533-545.

574 Pearson, F.J., Arcos, D., Bath, A., Boisson, J.Y., Fernandez, A.M., Gabler,
575 H.E., Gaucher, E., Gautschi, A., Griffault, L., Hernan, P., Waber, H.N., 2003. Mont
576 Terri project – Geochemistry of Water in the Opalinus Clay Formation at the Mont
577 Terri Rock Laboratory. Rapport de l'OFEG, Série Géologie, N°5 , Bern, 319p.

578 Ramambasoa, N., 2001. Etude du comportement hydromécanique des argilites:
579 Application au site de Tournemire. Thèse de l'Ecole Polytechnique.

580 Savoye, S., de Windt, L., Beaucaire, C., Bruno, G., Guitard, N., 2001. Are
581 artificial tracers conservative in argillaceous media ? The Tournemire claystone
582 case. In Cidu (Ed.), Water Rock Interaction proceedings 10, 1383-1386.

583 Savoye, S., Cabrera, J., Matray, J.M., 2003. Different hydraulic properties of
584 single fractures in argillaceous medium: the case of the IRSN Tournemire site
585 (France). IAH Conference IAH "Groundwaters in fractured rocks", Prague
586 (Tchéquie), sept 2003, Conference Proceeding, 47-50.

587 Savoye, S., Michelot, J.L., Wittebroodt, C., Altinier, M.V., 2006. Contribution
588 of the diffusive exchange method to the characterization of pore-water in
589 consolidated argillaceous rocks. J. Contam. Hydrol., in press.
590 Valès, F., Nguyen Minh, D., Gharbi, H., Rejeb, A., 2004. Experimental study of
591 the influence of the degree of saturation on physical and mechanical properties in
592 Tournemire shale (France). Appl. Clay Sci. 26, 197-207.
593 van Genuchten, M.T., 1980. A closed-form equation for predicting the
594 hydraulic conductivity of unsaturated soils. Soil Sci. Soc. Am. 44, 892-898.

595 Figure captions

596

597 Fig. 1. Geological cross section of the Tournemire URL.

598 Fig. 2. Hydraulic head profile through the argillaceous formation at Tournemire.

599 Fig. 3. Boreholes location and sections in the structural context of the Tournemire
600 URL.

601 Fig. 4. Schematic view of the MMPS device.

602 Fig. 5. Drillcore mapping, gas permeability and degree of saturation as a function
603 of the distance for boreholes MD2 and MD4 drilled from the drift 2003.

604 Fig. 6. Drill core mapping, gas permeability and degree of saturation as a function
605 of the distance for boreholes MD3 and MD5 drilled from the drift 1996.

606 Fig. 7. Drill core mapping, gas permeability and degree of saturation as a function
607 of the distance for boreholes MD6 and MD7 drilled from the century-old tunnel

608 Fig. 8. Comparison of modeled degrees of saturation with measured ones (A) in
609 borehole MD6 and (B) in borehole MD7.

610 Fig. 9. Comparison of modeled hydraulic with measured ones (A) in horizontal
611 direction and (B) in vertical direction. Only positive simulated hydraulic head
612 values were represented in the figure for clarity reasons and all negative ones were
613 fixed at zero.

Fig. 1

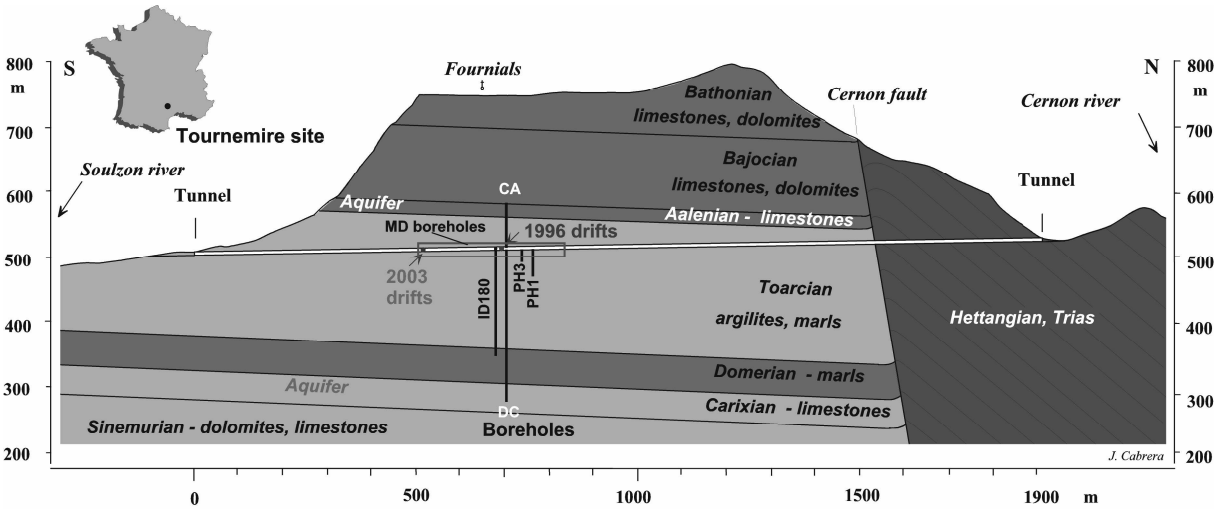
S
N
800 m
700
600
500
400
300
200
Tournemire site
Soulzon river
Tunnel
Fournials
Bathonian
limestones, dolomites
Cernon fault
Cernon river
Bajocian
limestones, dolomites
Aquifer
Aalenian - limestones
CA
MD boreholes
1996 drifts
2003
drifts
ID180
PH3
PH1
Toarcian
argilites, marls
Hettangian, Trias
Domerian - marls
Aquifer
Carixian - limestones
Sinemurian - dolomites, limestones
DC
Boreholes
J. Cabrera
0
500
1000
1500
1900 m

Fig. 2

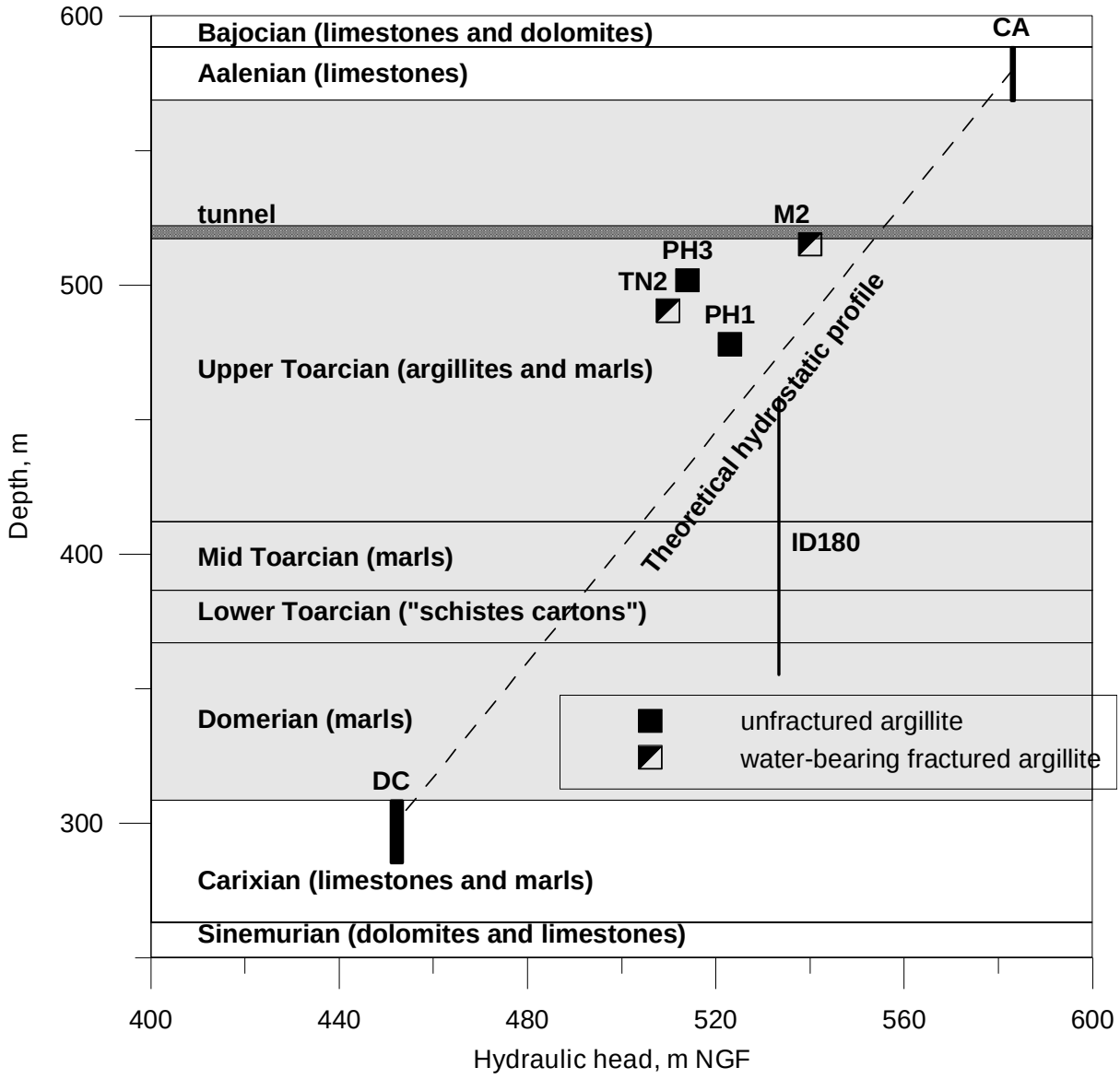
600
500
400
300
Depth, m
Bajocian (limestones and dolomites)
Aalenian (limestones)
tunnel
Upper Toarcian (argillites and marls)
Mid Toarcian (marls)
Lower Toarcian ("schistes cartons")
Domerian (marls)
Carixian (limestones and marls)
Sinemurian (dolomites and limestones)
CA
M2
PH3
TN2
PH1
DC
ID180
Theoretical hydrostatic profile
unfractured argillite
water-bearing fractured argillite
400
440
480
520
560
600
Hydraulic head, m NGF

Fig. 3

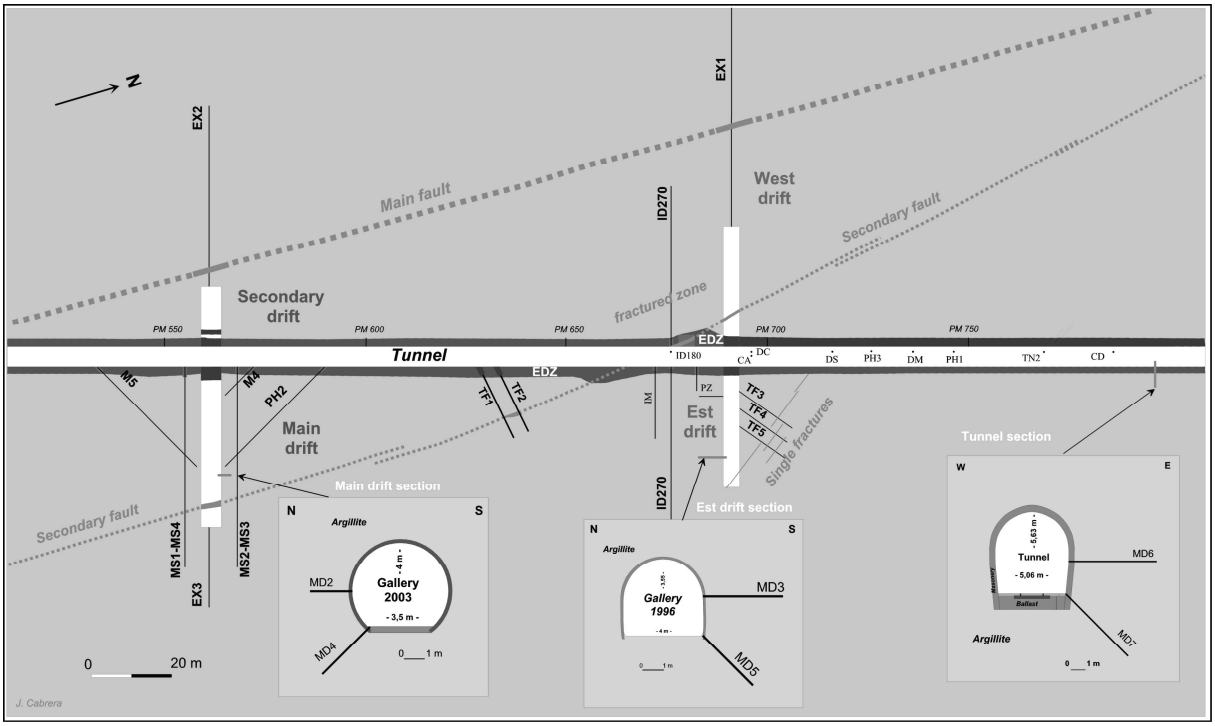
N
EX2
EX1
Main fault
West drift
ID270
Secondary fault
Secondary drift
fractured zone
PM 550
PM 600
PM 650
EDZ
PM 700
PM 750
Tunnel
ID180
CA
DC
DS
PH3
DM
PH1
TN2
CD
EDZ
M5
M4
PH2
TF1
TF2
IM
PZ
TF3
TF4
TF5
Est drift
Main drift
Single fractures
Tunnel section
Main drift section
Est drift section
Secondary fault
MS1-MS4
MS2-MS3
EX3
N
S
Argillite
MD2
Gallery 2003
- 3,5 m -
MD4
0 1 m
Gallery 1996
MD3
MD5
W
E
Tunnel
- 5,06 m -
MD6
MD7
Ballast
0 20 m
J. Cabrera

Fig. 4

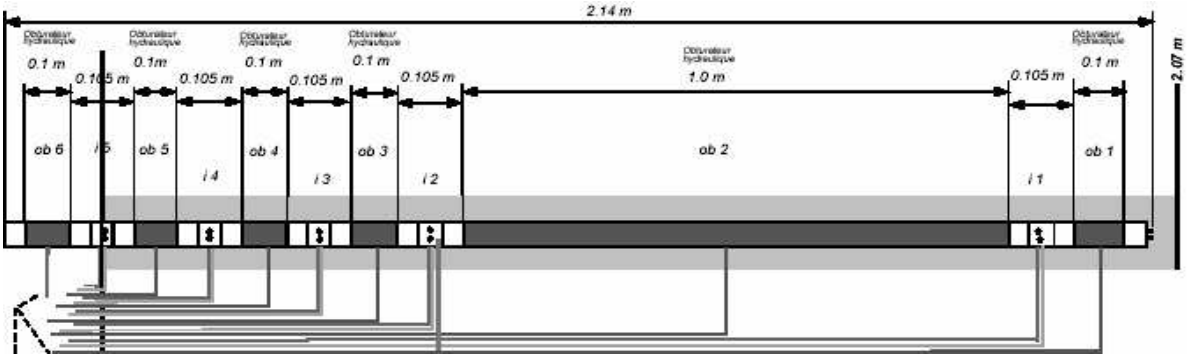
2.14 m
0.1 m
0.105 m
0.1m
0.105 m
0.1 m
0.105 m
0.1 m
0.105 m
1.0 m
0.105 m
0.1 m
2.07 m
ob 6
i 5
ob 5
i 4
ob 4
i 3
ob 3
i 2
ob 2
i 1
ob 1

Fig. 5

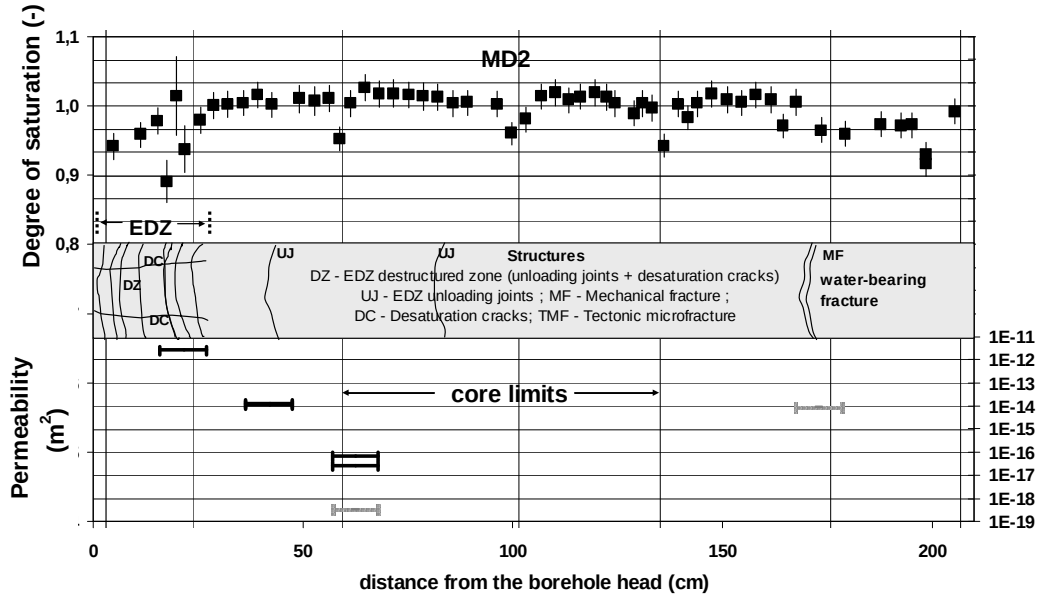
MD2
Degree of saturation (-)
1,1
1,0
0,9
0,8
EDZ
DC
DZ
DC
UJ
UJ
Structures
DZ - EDZ destructured zone (unloading joints + desaturation cracks)
UJ - EDZ unloading joints ; MF - Mechanical fracture ;
DC - Desaturation cracks; TMF - Tectonic microfracture
MF
water-bearing fracture
Permeability (m2)
core limits
1E-11
1E-12
1E-13
1E-14
1E-15
1E-16
1E-17
1E-18
1E-19
0
50
100
150
200
distance from the borehole head (cm)

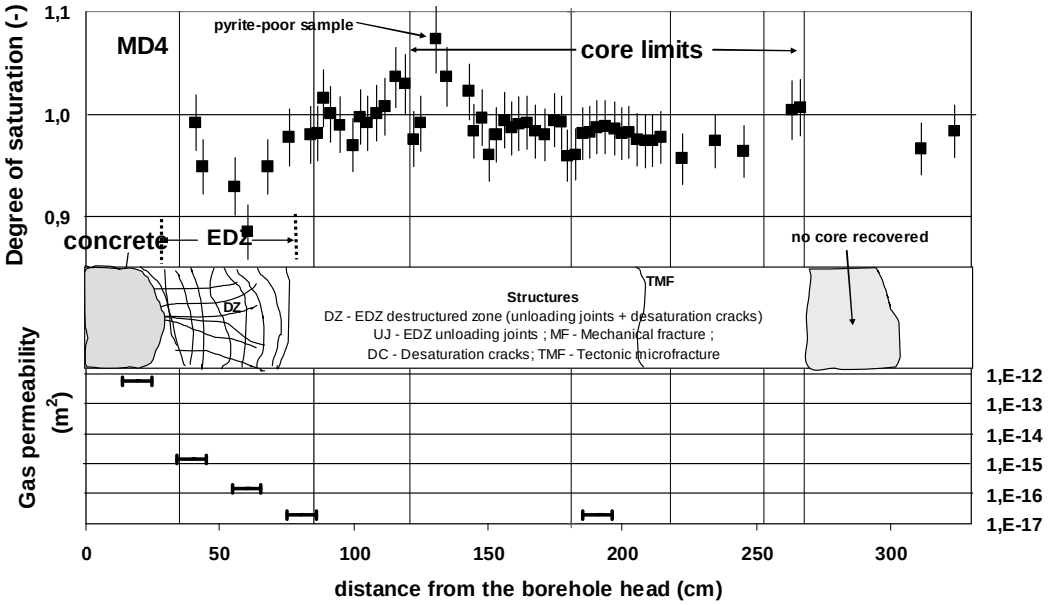
MD4
pyrite-poor sample
core limits
Degree of saturation (-)
1,1
1,0
0,9
concrete
EDZ
no core recovered
DZ
TMF
Structures
DZ - EDZ destructured zone (unloading joints + desaturation cracks)
UJ - EDZ unloading joints ; MF - Mechanical fracture ;
DC - Desaturation cracks; TMF - Tectonic microfracture
Gas permeability (m2)
1,E-12
1,E-13
1,E-14
1,E-15
1,E-16
1,E-17
0
50
100
150
200
250
300
distance from the borehole head (cm)

Fig. 6

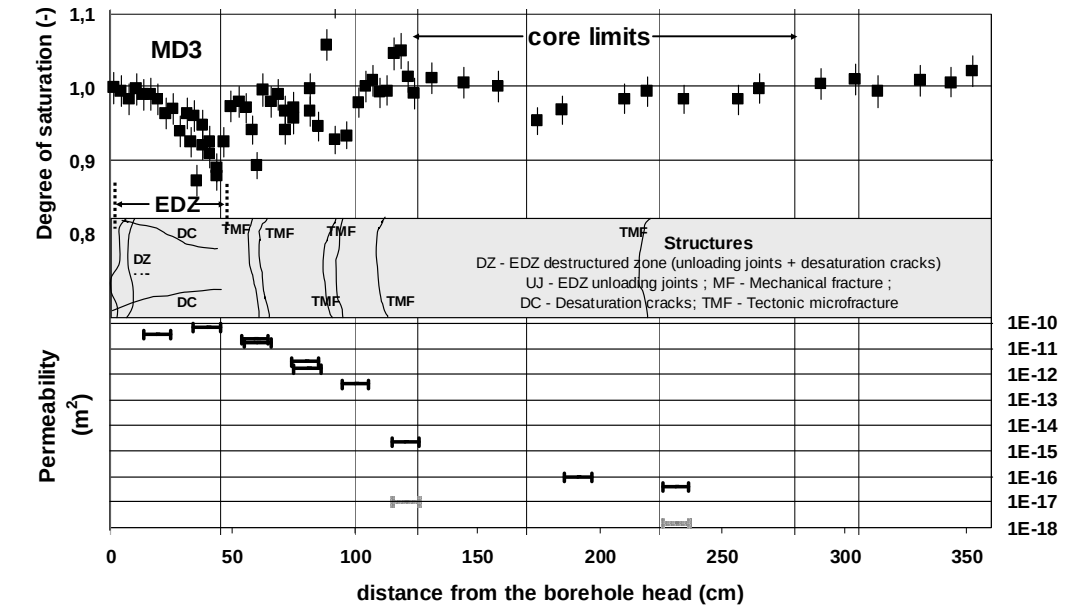
MD3
core limits
Degree of saturation (-)
1,1
1,0
0,9
0,8
EDZ
DC
DZ
DC
TMF
TMF
TMF
TMF
TMF
TMF
Structures
DZ - EDZ destructured zone (unloading joints + desaturation cracks)
UJ - EDZ unloading joints ; MF - Mechanical fracture ;
DC - Desaturation cracks; TMF - Tectonic microfracture
Permeability (m2)
1E-10
1E-11
1E-12
1E-13
1E-14
1E-15
1E-16
1E-17
1E-18
0
50
100
150
200
250
300
350
distance from the borehole head (cm)

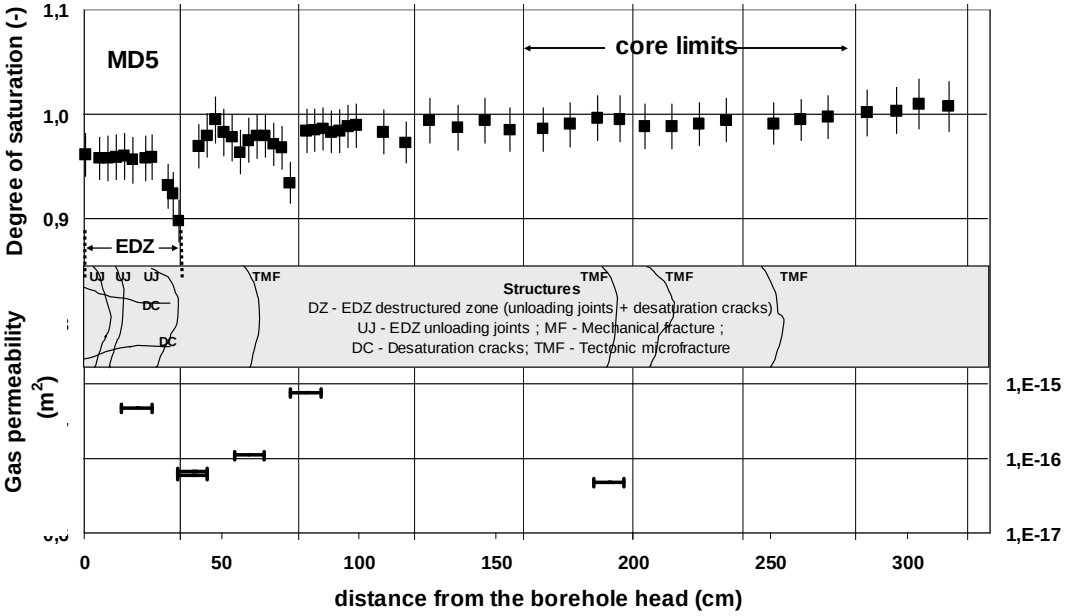
MD5
core limits
Degree of saturation (-)
1,1
1,0
0,9
EDZ
UJ
UJ
UJ
DC
DC
TMF
TMF
TMF
TMF
Structures
DZ - EDZ destructured zone (unloading joints + desaturation cracks)
UJ - EDZ unloading joints ; MF - Mechanical fracture ;
DC - Desaturation cracks; TMF - Tectonic microfracture
Gas permeability (m2)
1,E-15
1,E-16
1,E-17
0
50
100
150
200
250
300
distance from the borehole head (cm)

Fig. 7

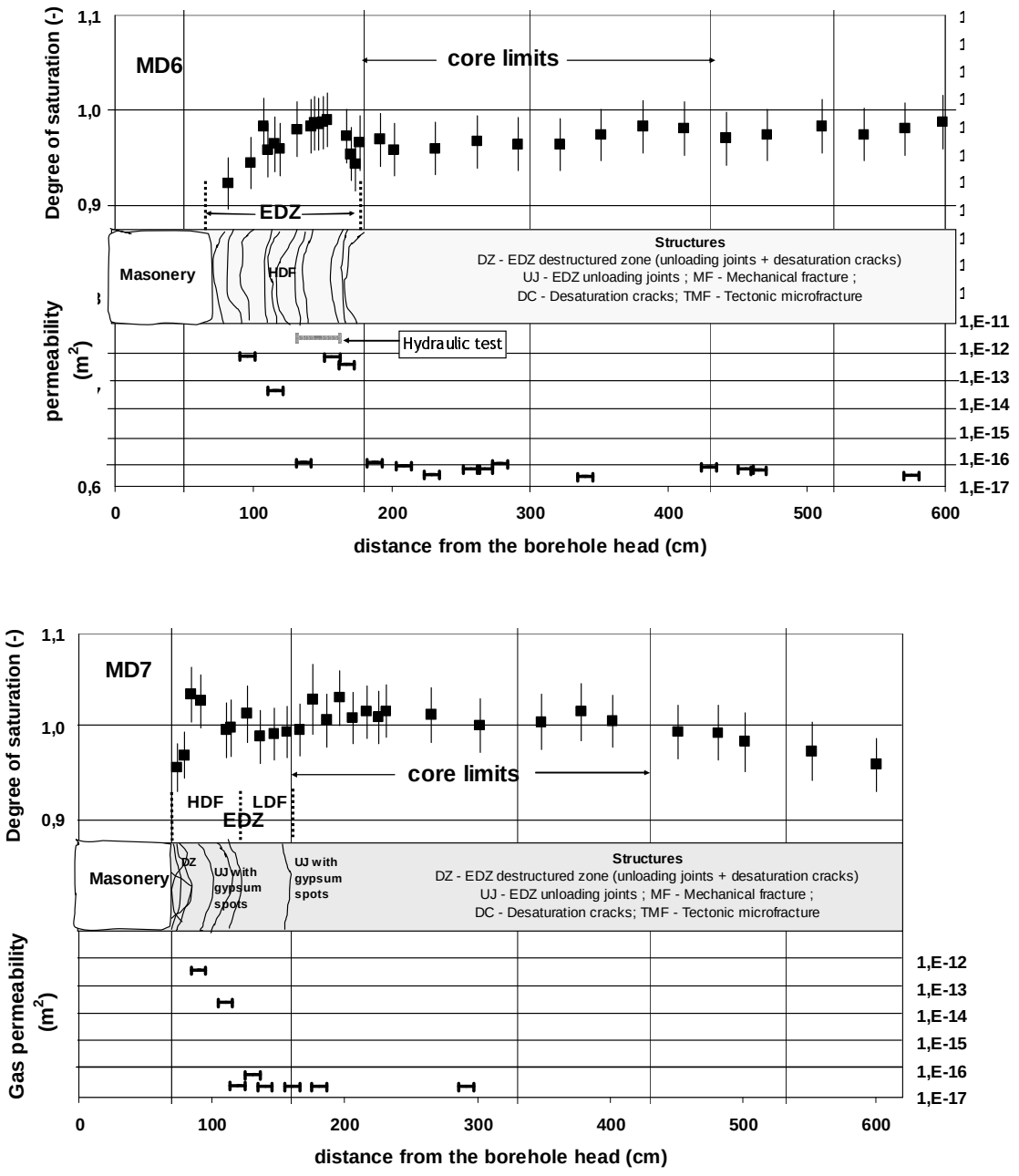
MD6
core limits
EDZ
Degree of saturation (-)
1,1
1,0
0,9
0,6
Masonery
HDF
Structures
DZ - EDZ destructured zone (unloading joints + desaturation cracks)
UJ - EDZ unloading joints ; MF - Mechanical fracture ;
DC - Desaturation cracks; TMF - Tectonic microfracture
Hydraulic test
permeability (m²)
1,E-11
1,E-12
1,E-13
1,E-14
1,E-15
1,E-16
1,E-17
0
100
200
300
400
500
600
distance from the borehole head (cm)
MD7
core limits
HDF
LDF
EDZ
Degree of saturation (-)
1,1
1,0
0,9
Masonery
DZ
UJ with gypsum spots
UJ with gypsum spots
Structures
DZ - EDZ destructured zone (unloading joints + desaturation cracks)
UJ - EDZ unloading joints ; MF - Mechanical fracture ;
DC - Desaturation cracks; TMF - Tectonic microfracture
Gas permeability (m²)
1,E-12
1,E-13
1,E-14
1,E-15
1,E-16
1,E-17
0
100
200
300
400
500
600
distance from the borehole head (cm)

Fig. 8 (A) and (B)

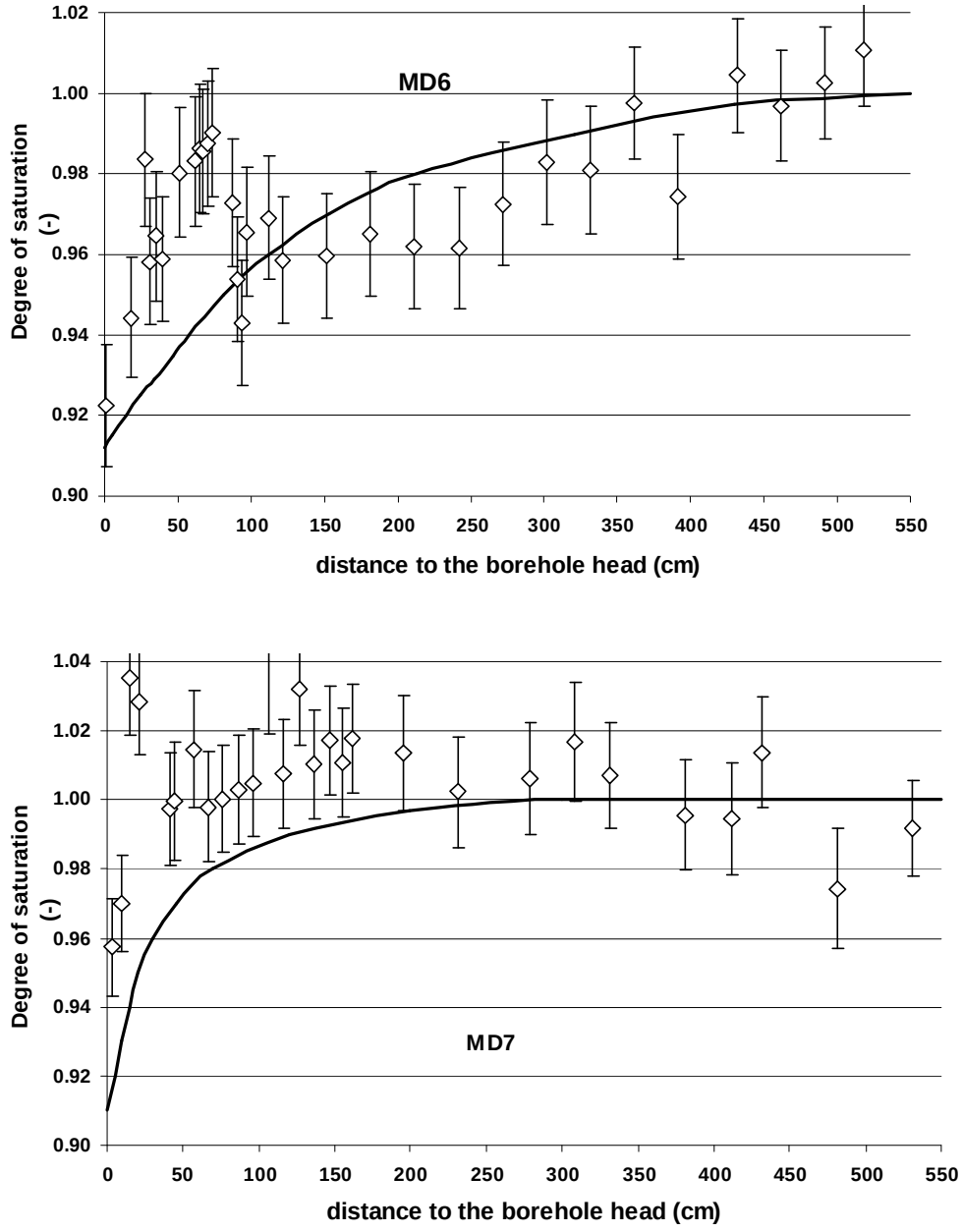
MD6
Degree of saturation (-)
1.02
1.00
0.98
0.96
0.94
0.92
0.90
0
50
100
150
200
250
300
350
400
450
500
550
distance to the borehole head (cm)
MD7
Degree of saturation (-)
1.04
1.02
1.00
0.98
0.96
0.94
0.92
0.90
0
50
100
150
200
250
300
350
400
450
500
550
distance to the borehole head (cm)

Fig. 9 (A) and (B)

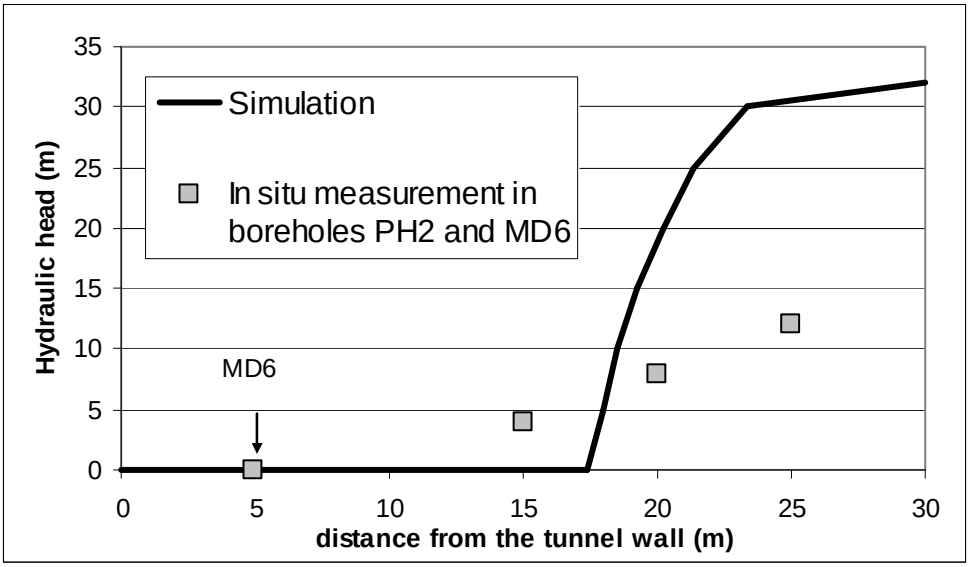
Simulation
In situ measurement in boreholes PH2 and MD6
MD6
Hydraulic head (m)
distance from the tunnel wall (m)
0
5
10
15
20
25
30
35

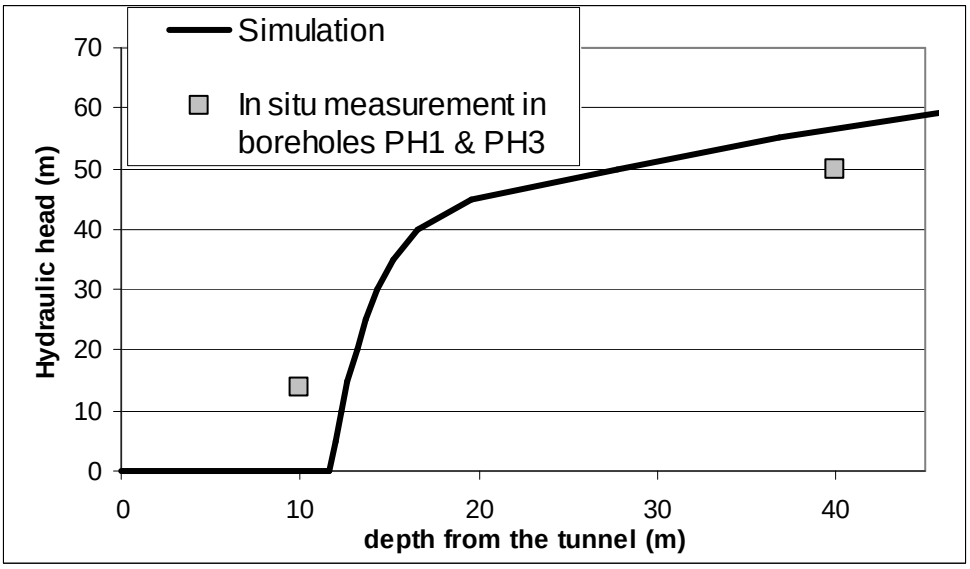
Simulation
In situ measurement in boreholes PH1 & PH3
Hydraulic head (m)
depth from the tunnel (m)
0
10
20
30
40
50
60
70

Table 1

Main objectives (C for petrophysical measurements, H hydraulic tests, P pneumatic tests) and characteristics of boreholes realized in the framework of this study. Section A, B and C refers respectively to gallery 2003, gallery 1996 and century-old tunnel.

ID /section	Aim	Date	Drift (distance from the tunnel)	Azimuth	Dip angle	Length	Height of borehole head/ ground
					Degree	*m*	*m*
MD2 /A	C/H /P	29/06/04	Drift 2003 (27m N wall)	N15	0° sub parallel to bedding	2.07	1.6
MD3 /B	C/H /P	12/10/04	Drift 1996 (23m)	N195	0° sub parallel to bedding	3.58	1.5
MD4 /A	C/P	22/11/04	Drift 2003 (27m)	N15	45° down	3.41	1.6
MD5 /B	C/P	23/11/04	Drift 1996 (23m)	N15	45° down	3.22	1.5
MD6 /C	C/H /P	23/02/05	Tunnel 1885	N105	0° sub parallel to bedding	6.00	1.87
MD7 /C	C/P	22/02/05	Tunnel 1885	N105	45° down	6.00	1.87

Table 2

Average values of water content, total porosity, volumetric moisture content and degree of saturation determined Inside and Outside the EDZ areas.

Borehole	EDZ	$WC_{dry,150°}$, %	n_{tot}, %	θ, %	S, %
MD2	In	3.073 ± 0.003	7.79 ± 0.18	7.612 ± 0.38	97.7 ± 2.7
MD2	Out	4.085 ± 0.003	9.92 ± 0.18	9.93 ± 0.37	100.1 ± 1.8
MD3	In	3.284 ± 0.007	8.53 ± 0.18	8.14 ± 0.65	95.1 ± 2.1
MD3	Out	3.562 ± 0.005	8.87 ± 0.18	8.77 ± 0.65	98.9 ± 2.5
MD4	In	3.891 ± 0.021	9.95 ± 0.28	9.51 ± 0.64	95.2 ± 2.7
MD4	Out	4.150 ± 0.005	10.07 ± 0.27	10.06 ± 0.63	100.1 ± 2.7
MD5	In	3.180 ± 0.004	8.31 ± 0.18	7.91 ± 0.38	94.9 ± 2.1
MD5	Out	3.456 ± 0.004	8.67 ± 0.18	8.53 ± 0.37	98.6 ± 2.1
MD6	In	3.670 ± 0.003	9.29 ± 0.27	9.04 ± 0.64	96.9 ± 2.8
MD6	Out	3.704 ± 0.003	9.38 ± 0.27	9.11 ± 0.65	97.0 ± 2.8
MD7	In	3.910 ± 0.003	9.60 ± 0.27	9.57 ± 0.64	99.7 ± 2.8
MD7	Out	3.783 ± 0.004	9.26 ± 0.27	9.29 ± 0.64	100.3 ± 2.9